50272-101

REPORT DOCUMENTATION PAGE	1. REPORT NO. NSF-RA-E-75-280	2.	PB 286 744

4. Title and Subtitle

Experimental Study of Concrete Masonry Under Seismic-Type Loading

5. Report Date 1975

6.

7. Author(s)

G.A. Hegemier, G. Krishnamoorthy, and R.O. Nunn

8. Performing Organization Rept. No.

9. Performing Organization Name and Address

University of California
Department of Applied Mechanics and Engineering Sciences
P. O. Box 109
La Jolla, California 92037

10. Project/Task/Work Unit No.

11. Contract(C) or Grant(G) No.

(C)

(G) 74-14818

12. Sponsoring Organization Name and Address

Applied Science and Research Applications (ASRA)
National Science Foundation
1800 G Street, N.W.
Washington, D.C. 20550

13. Type of Report & Period Covered

14.

15. Supplementary Notes

16. Abstract (Limit: 200 words)

An experimental study is outlined to define material rheology for concrete masonry under seismic-type loading for the development of a basis for a rational earthquake response and damage analysis. Elementary experiments on the basic constituents of concrete masonry and their interactions are conducted. Homogeneous and nonhomogeneous biaxial tests of panels under both quasistatic and dynamic cyclic load histories are carried out. The above is complemented by tests on typical connections to be discussed in a companion paper. The sequence culminates with studies of major structural elements. The ability to extrapolate from conceptually simple laboratory scale experiments to a wide variety of structural configurations, including full-scale building response to earthquake ground motion, is one of the most significant aspects of the project. It is pointed out that masonry is some 20 years or more behind concrete with respect to knowledge of material properties and that absence of comprehensive knowledge in this area can only invite potentially enormous safety and economic problems.

17. Document Analysis a. Descriptors

Experimentation
Concrete products
Masonry
Concrete construction
Concretes
Concrete blocks
Construction materials
Earthquake resistant structures

b. Identifiers/Open-Ended Terms

c. COSATI Field/Group

18. Availability Statement	19. Security Class (This Report)	;es
NTIS.	20. Security Class (This Page)	22. Price PC A03

AN EXPERIMENTAL STUDY OF CONCRETE MASONRY UNDER SEISMIC - TYPE LOADING

by

G. A. Hegemier[1], G. Krishnamoorthy[2], R. O. Nunn[3]

ABSTRACT

This paper outlines portions of a comprehensive research program on concrete masonry. Objectives, scope, methodology, and sample results obtained to date are presented. Where appropriate, practical implications of the latter are delineated. Future experiments are discussed.

I. INTRODUCTION

1.1 The Program

The development of a basis for a rational earthquake response and damage analysis of concrete masonry structures is the subject of an extensive experimental, analytical, and numerical research program at the San Diego campus of the University of California. The program is sponsored by the National Science Foundation under project RANN.

The experimental effort is intended to define material rheology. The analytical phase involves the translation of observed experimental data into viable mathematical models. The numerical effort concerns the conversion of mathematical models into numerical form and the construction of digital computer codes to simulate structural response and damage accumulation resulting from earthquake ground motion.

Discussion in this paper is confined to the experimental portion of the program.

---

[1]Professor, Dept Appl Mechs & Engr Sci, University of California, San Diego, La Jolla, California, 92093.

[2]Professor, Dept Civil Engr, San Diego State University, San Diego, California, 92182.

[3]Graduate Student, Dept Appl Mechs & Engr Sci, University of California, San Diego, La Jolla, California, 92093.

1.2 The Approach

The approach selected to achieve the project objectives involves a sequence of increasingly complex levels of concurrent experimentation, analysis, and numerical simulation. This sequence begins with elementary experiments on the basic constituents of concrete masonry and their interactions, e g, by fracture and slip across interfaces. It proceeds to homogeneous and nonhomogeneous biaxial tests of panels under both quasi-static and dynamic cyclic load histories. The above is complemented by tests on typical connections (to be discussed in a companion paper). The sequence culminates with studies of major structural elements. The ability to extrapolate from conceptually simple laboratory scale experiments to a wide variety of structural configurations, including full-scale building response to earthquake ground motion, is one of the most significant aspects of the project.

1.3 The Need for Research

Comprehensive surveys of the available literature relevant to the mechanics of concrete masonry assemblies can be found in references [1, 2]. Examination of these reports reveals that, although a measurable amount of research on concrete masonry has been conducted over the past forty to fifty years, there currently exists little correlation among the various studies conducted by governmental, university, and promotional research organizations. Each study has, of economic necessity and/or impatience, been constrained within narrow bounds and primarily to specific structural configurations rather than to fundamental material research. As a result, a virtual vacuum exists concerning the material properties of concrete masonry, and the behavior of typical connections used in concrete masonry systems. In the absence of reliable data, subjective judgement must be substituted for a rational analysis. The ramifications of this substitution are obvious and clearly undesirable. The present program constitutes a major step in the direction of alleviating the above problem.

II. MATERIAL TEST PROGRAM - DESCRIPTION

2.1 Basic Items Under Study

The basic experimental items under current study concern planar material behavior and are related to the construction of constitutive relations for concrete masonry in both linear and nonlinear ranges. Included are:

- Strength and damage accumulation under combined plane-stress states
- Stiffness parameters
- Energy absorption and damping

In each of the above areas, studies are well underway to determine the:

- Degree of anisotropy
- Degree of strain-rate sensitivity
- Influence of reinforcing steel
- Influence of compaction (vibration)
- Influence of admixtures
- Influence of flaws
- Influence of constituent properties on assembly properties
- Scale effects
- Degradation under cyclic load histories

2.2 Methodology

The program partitions naturally into two main categories: (1) Small-scale or "microelement" tests and (2) Large-scale or "macroelement" tests.

The objective of the small-scale tests is to synthesize the behavior or properties of masonry assemblies or macroelements from simple but universal experiments - experiments that can be conducted in a standard laboratory. At the very least such tests provide an index concerning the influence of the basic constituents on assembly behavior.

The large-scale or macroelement tests constitute a necessary check on the micro-modeling process and, perhaps more important, constitute the starting point for the

construction of a continuum model of concrete masonry. The latter, it is anticipated, may be used to efficiently synthesize the behavior of complex structures, in combination with appropriate connection data, through the use of explicit analytical and numerical techniques.

The overall methodology is depicted in Fig 1.

2.3 Materials

Two nominal[4] masonry types are currently under study: (1) "normal strength" - type N normal weight concrete block (ASTM C90), type S mortar (ASTM C270), 2000 psi coarse (pump mix, 8-10 inch slump) grout (ASTM C476); (2) "high strength" - light-weight block ($f'_c \geq 3750$ psi, type M mortar (ASTM C270), 3750 psi coarse (pump mix, 8-10 inch slump) grout (ASTM C476).

Most specimens consist of running bond with face-shell bedding. Both closed and open-end units are utilized, although focus is currently on the former. Standard 8-inch high, 8-inch wide block geometries [1] are employed.

2.4 Small-Scale Tests

Testing and modeling on the micro-scale commences at the constituent level and requires a knowledge of constituent, constituent-interface and small assembly behavior under various stress states.

Constituent tests serve as index factors for each test series (micro or macro). Test data includes elastic moduli, compressive strength, and tensile strength of block, grout, and mortar. Information on unit-absorption, and design mixes for each component is also obtained.

Joint tests are of considerable interest. Joints or interfaces in concrete masonry assemblies constitute both planes of weakness and a major source of damping. Failures

---

[4] Precise details concerning material properties are provided in appropriate sections to follow.

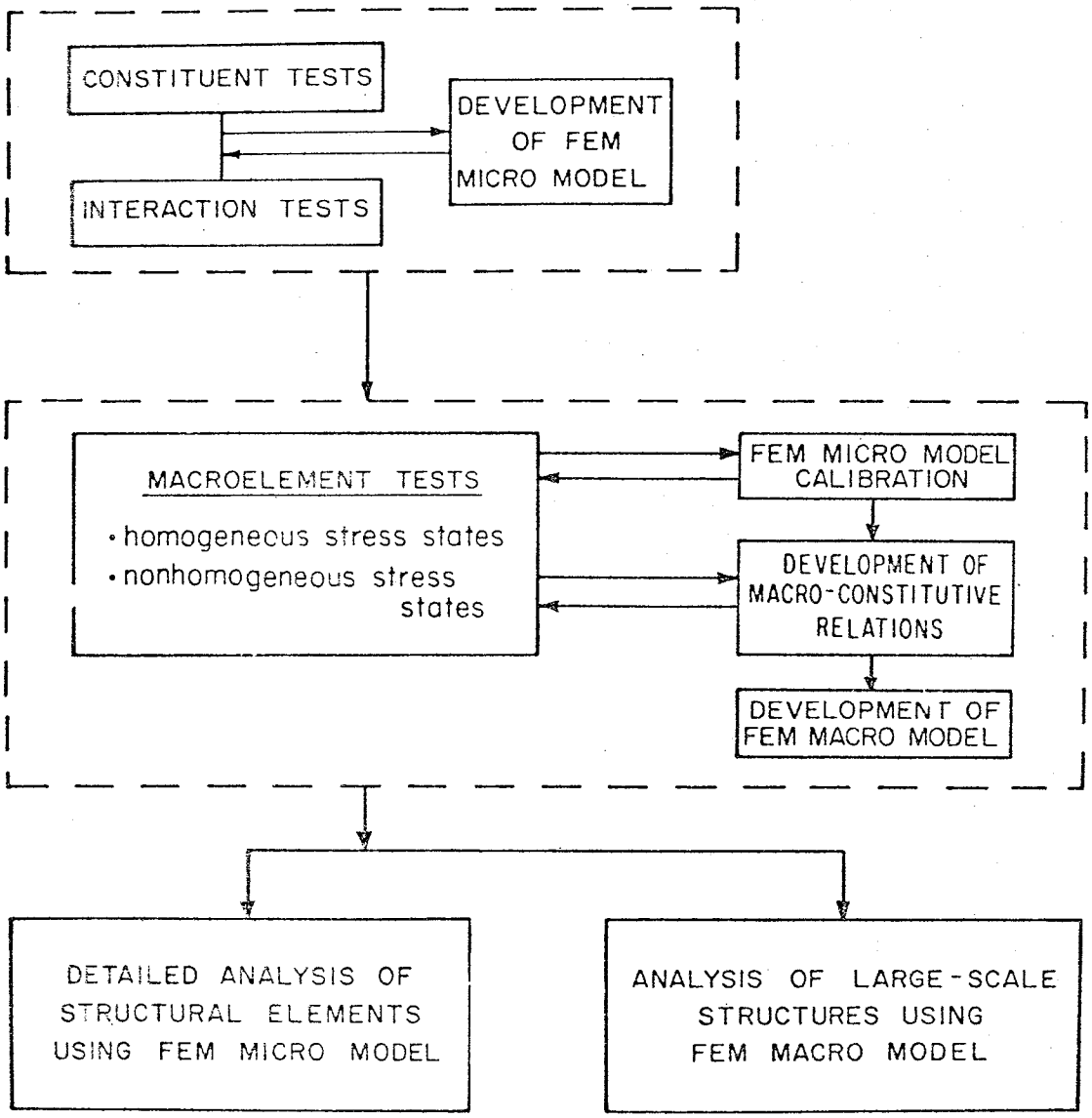

Fig. 1 Methodology of Research Program.

frequently initiate in joints, and subsequent deformation and energy absorption may occur by relative slip across joint planes. Joint types selected for study include: (1) ungrouted bed joints; (2) grouted bed joints with and without steel; (3) head joints; (4) combination head and bed joints; (5) and block-grout interfaces. Mortar geometry includes both full and face-shell bedding. Test specimens in the joint-series consist primarily of triplets (three blocks, two interfaces). Six inch cores are utilized for block-grout interface tests. Joint planes are subjected to constant levels of normal stress and quasi-static monotonic, quasi-static cyclic, or dynamic cyclic shear stress. In each test the initial and post-fracture shear-stress vs normal stress envelopes, and deformation histories, are determined.

In addition to the above, a variety of prism (small assembly) tests are well underway. These tests are designed to provide basic information on: (1) the influence of the number of courses on compressive strength and associated problems regarding load-platen restraint; (2) the influence of flaws, compaction, and admixtures on compressive and tensile strength; (3) the correlation of compressive and tensile strengths; (4) correlation of block, grout, and mortar strengths to prism strengths; (5) stiffness parameters and uniaxial stress-strain behavior (these include Young's modulus in tension, Young's modulus in compression, ratio of tensile to compressive strengths, ratio of tensile strength to tensile modulus, ratio of compressive strength to compressive modulus).

2.5 Static and Dynamic Biaxial Panel Tests

As was noted previously, modeling on the continuum or macro-scale, and calibration of micro-models, is acccomplished via biaxial panel tests of two basic stress state types: homogeneous and nonhomogeneous. The specimens in this test series are approximately one order of magnitude larger than the typical microdimension.

2.5.1 Globally Homogeneous Stress-States

These tests are unique in that the panels are laid in running bond, but are saw-cut such that the bonds run at oblique incidence or layup to the edges of the finished panel. The rationale: any combination of homogeneous shear and normal stresses on the critical bed and head joint planes can be induced by application of direct (principal) stresses (compression or tension) to panel edges, and the selection of a proper layup angle. The ability to apply direct tensile stresses which exceed the tensile strength of the assembly, and direct compressive stresses with negligible induced shear, follows from the use of a unique polysulfide bonding agent with a low shear modulus ($\simeq$ 150 psi) between the specimen and the load distribution fixtures. In the case of uniform load application to each panel edge, the resulting panel stress distribution is globally homogeneous, and hence statically determinate. Thus, in contrast to conventional test methods [2], the determination of material properties is not prejudiced by ·dary constraints; further, in contrast to indirect methods [1], extraction of biaxial failure states does not necessitate a conjecture of isotropic, linear elastic material behavior prior to macrocracking.

Figure 2 illustrates the basic concept of oblique layup testing. If the x_1, x_2 - axes are principal stress directions, then the stress resultants[5] N_{11}', N_{22}', N_{12}' associated with axes x_1', x_2' along the bed and head joint directions are related to the principal stress resultants N_{11}, N_{22} through

$$N_{11}', N_{22}' = \frac{N_{11} + N_{22}}{2} \pm \frac{N_{11} - N_{22}}{2} \cos 2\theta \ , \ N_{12}' = \frac{N_{22} - N_{11}}{2} \sin 2\theta \qquad (1)$$

Equations (1) imply that any homogeneous stress-state (N_{11}', N_{22}', N_{12}') in a panel with surfaces oriented parallel to the head and bed joints can be obtained by selecting an appropriate layup angle θ and direct stress resultants N_{11}, N_{22}. In particular, given a desired stress-state (N_{11}', N_{22}', N_{12}'), the combination (N_{11}, N_{22}, θ) is selected according to

---

[5] Stress resultants are related to stress by $\sigma_{ij} = N_{ij}/t$, where t is the panel thickness.

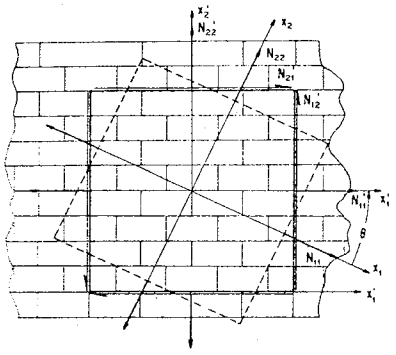

Fig. 2 Stress Transformation.

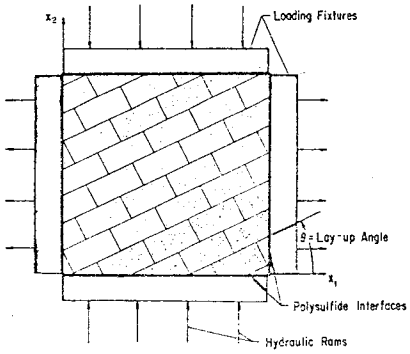

Fig. 3 Loading Schematic.

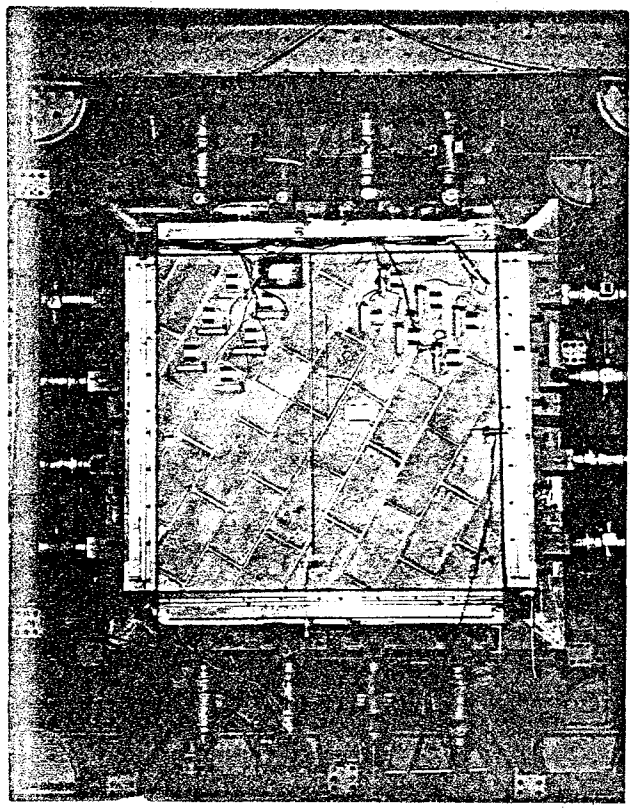

Fig. 4 Biaxial Fixture.

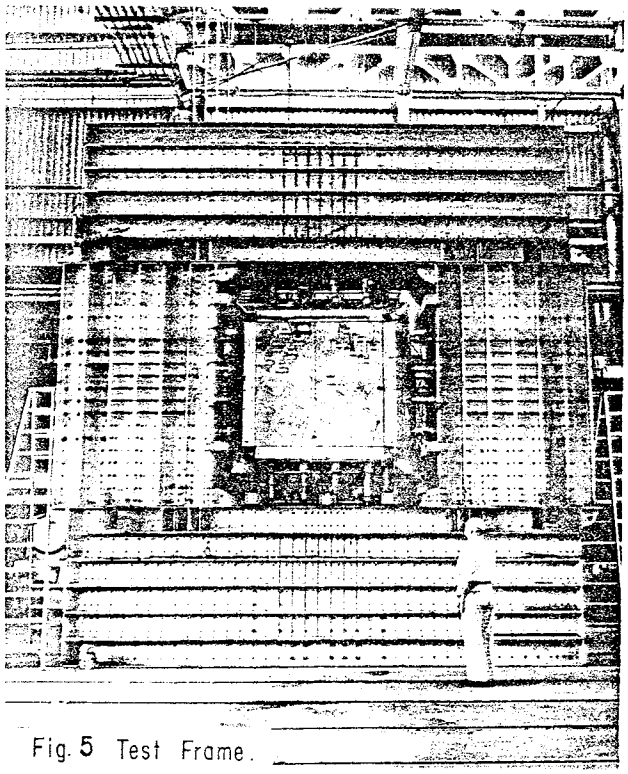

Fig. 5 Test Frame.

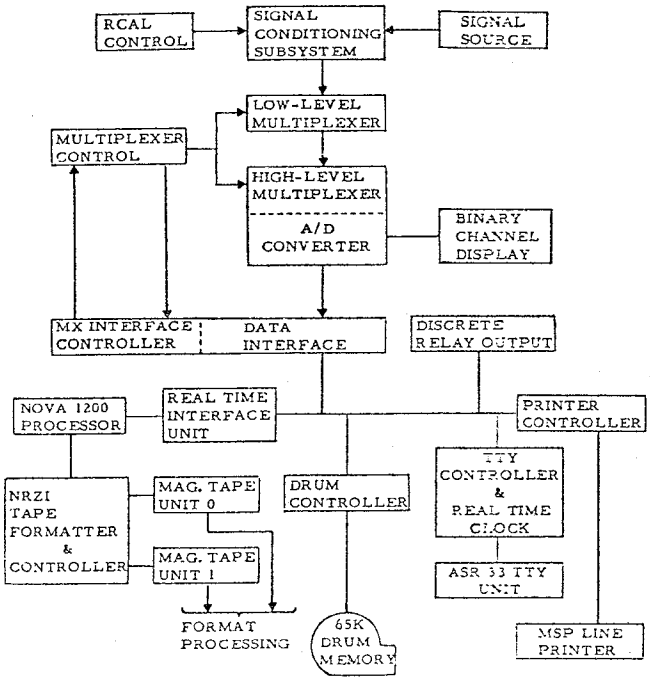

Fig. 6 Data Acquisition.

$$N_{11},\ N_{22} = \frac{N_{11}' + N_{22}'}{2} \pm \frac{N_{11}' - N_{22}'}{2} \cos 2\theta \mp N_{12}' \sin 2\theta$$

$$\tan 2\theta = -2N_{12}'/(N_{11}' - N_{22}') \qquad (2)$$

The test panels of 64-by-64 inches are precision cut from 8-by-8 foot fully grouted, unreinforced or reinforced concrete masonry walls constructed to current field practice. Cutting is accomplished by use of a dynamically balanced, 30-inch-diameter, diamond-edge saw on an air-driven turbine. The above panel size constitutes the smallest specimen deemed to be a macroelement, i e, such that the minimum panel (planar) dimension is one order of magnitude greater than the largest microelements (block units).

A schematic of the biaxial test procedure is shown in Fig 3. The actual setup is illustrated in Fig 4. The load conditions include quasi-static monotonic, quasi-static cyclic, and dynamic cyclic (.05 to 5Hz). The system is capable of load, displacement, or combined load-displacement control. This is accomplished with a mini-computer-controlled, closed-loop-hydraulic-servo system utilizing four active actuators on each panel side connected to load distribution fixtures. This test system is housed in a massive dual test frame, Fig 5. A high-speed digital data acquisition system (14 bits absolute value plus sign, 300 samples/sec/channel or 15,000 samples/sec total), Fig 6, monitors 40 channels of signals from load cells, linear variable differential transformers (LVDT's), and strain gages.

Rheological aspects of singular interest include: (1) elastic properties; (2) degree of anisotropy of elastic properties; (3) damping or stress-strain hysteresis in the "elastic" regime; (4) strain-rate sensitivity of item 3, above, in the .05 to 4Hz range; (5) initial "yield" or macro-fracture surface in stress-space; (6) degree of anisotropy of item 5 above; (7) ultimate strength; (8) influence of load history on the degradation of stiffness and ultimate strength; (9) hysteresis in the highly nonlinear range; (10) role of reinforcing steel geometry and volume in the control of macrocracking; and (11) flaw sensitivity.

2.5.2 Nonhomogeneous Stress-States

The significance of these tests is as follows. Homogeneous stress-state tests, as described in the previous section, assume that characteristic lengths associated with variation in the stress field are large when compared with the typical microdimensions of the material. In plain concrete this rarely presents a problem[6] since the typical microdimension is associated with the largest aggregate dimension, which in turn is small. In concrete masonry, on the other hand, the typical microdimension is quite large-8 to 16 inches (the block size). Thus, the typical microdimension of this material may not be small where compared with either the structural-element size or the characteristic length of the stress field. In such a case it is necessary to create a material model which, to a certain degree of accuracy, reflects the influence of the microstructure. Nonhomogeneous stress-state tests are a necessary step in this process. They comprise an advanced step in the micromodeling process, and a first evaluation of the limits of application of the macro or continuum modeling process, and modification of the latter to reflect microstructural effects.

The tests in this series consist of two types: (1) simple shear deformation and (2) diagonal compression. A brief discussion of each is presented below.

2.5.2.1 Simple Shear Deformation

The test system described above, as modified according to Fig 7, and with a modified bonding agent, is capable of creating simple shear deformation (in contrast to pure shear stress) - with superposed axial deformation or stress. Such tests, to be conducted on 0 degree layup specimens only, mirror the behavior of shear walls and piers under varying degrees of end constraint. Consequently, this test-type serves to calibrate all modeling in a region of primary interest. The rheological items of interest here are similar to those listed under Section 2.5.1.

---

[6] It does present a problem in reinforced concrete.

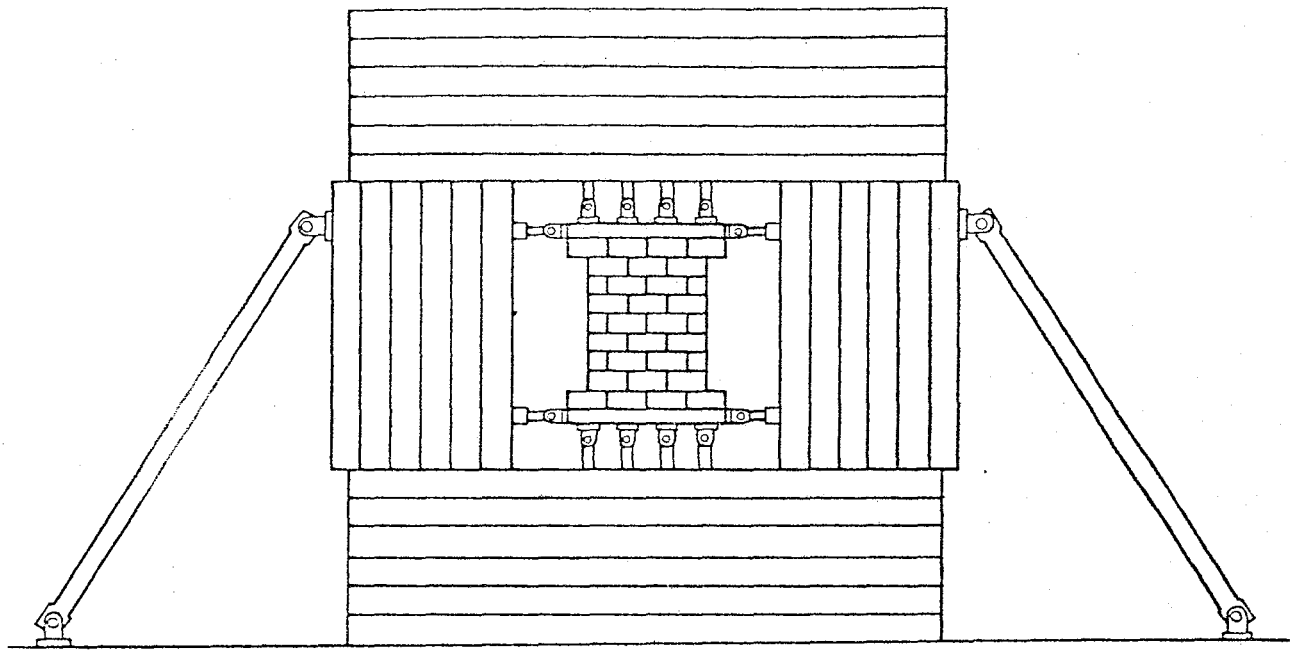

Fig. 7 Panel Shear Test.

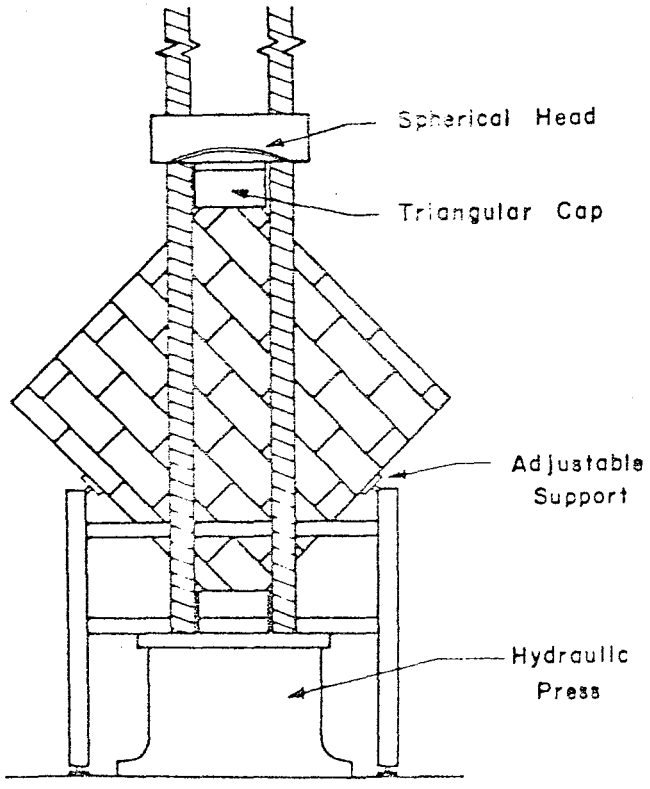

Fig. 8 Diagonal Compression Test.

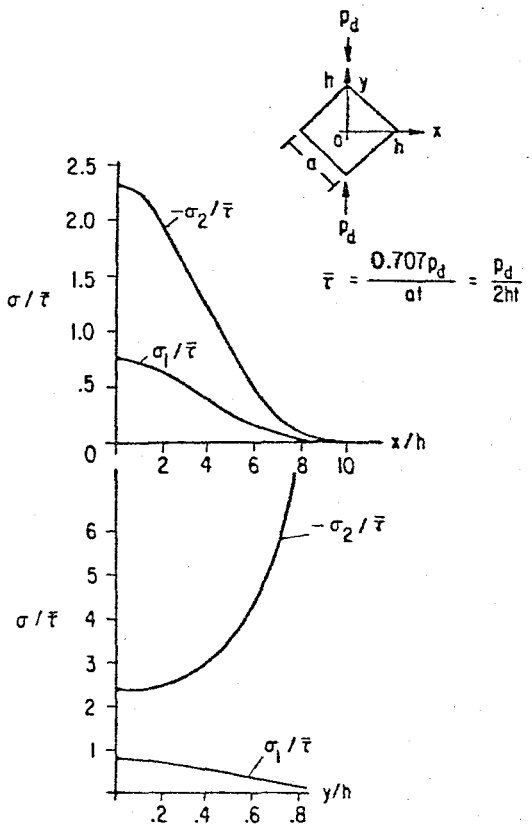

Fig. 9 Diagonal Compression Test: Principal Stress Distribution on the Planes $y = 0$ and $x = 0$.

2.5.2.2 Diagonal Compression

This test, which is illustrated in Fig 8, is actually an indirect biaxial test [1]. Under concentrated diagonal compressive loads, the central portion of the specimen is subjected to a biaxial stress-state which is reasonably uniform over a characteristic length (area). This length, however, is not large where compared to the material micro-dimensions; hence the test constitutes a simple check on the limits of application of the homogeneous failure data obtained from the tests of Section 2.5.1.

The above test, by the way, is greatly misunderstood in the literature. Most documents interpret the test results incorrectly (e g, see ASTM E519-74). It is not a shear test; the shear stress on the planes intersecting diagonals vanishes from symmetry. Failure occurs by induced tensile stresses on the vertical plane of symmetry (see Fig 9).

III. MATERIAL TEST PROGRAM - SUMMARY

For the convenience of the reader, the material test program discussed in the previous section is summarized below.

3.1 Constituent Tests

- Compressive and tensile strength of grout, mortar, block
- Shear and tensile strength of bonds or interfaces
- Elastic moduli of block, grout, mortar
- Absorption of units

3.2 Prism Tests

- Influence of number of courses on compressive strength
- Influence of flaws on compressive and tensile strengths
- Influence of compaction and admixtures on compressive and tensile strengths
- Correlation of compressive and tensile strengths
- Correlation of block, grout, and mortar strengths to prism strengths

- Stiffness parameters and uniaxial stress-strain behavior (Young's modulus in tension and compression, ratio of tensile strength to compressive strength, ratio of tensile strength to tensile modulus, ratio of compressive strength to compressive modulus)

3.3 Interface Tests

- Strength of ungrouted bed joints
- Strength of grouted bed joints
- Strength of head joints
- Post fracture slip-behavior of joints
- Influence of steel on joint properties
- Block-grout interface strength

3.4 Full Scale Tests (Homogeneous stress states)

- Biaxial failure envelopes (Degree of anisotropy, influence of flaws, influence of compaction, influence of admixtures, influence of steel)
- Post macrocracking hysteretic behavior (reinforced specimens only)
- Elastic moduli (Young's modulus, Poisson's ratio, degree of anisotropy)
- Damping and energy absorption
- Prediction of failure and elastic properties from small-scale tests; scale effects

3.5 Full Scale Tests (Nonhomogeneous stress states)

- Simple shear deformation - monotonic and cyclic loading (stiffness degradation, energy absorption, ultimate failure, general hysteretic behavior)
- Diagonal compression test (significance, correlation with biaxial failure data)

IV. SELECTED RESULTS - PANELS

The purpose of this section is to present sample results obtained to date under this program. The discussion is intended for illustrative purposes only, and is confined to basic features of experimental data. Design recommendations are not made herein; the

latter must await completion of appropriate test series, comprehensive data reduction, data interpretation and case studies.

A complete description of the biaxial tests is beyond the scope of this presentation. For simplicity, attention is focused below upon the homogeneous stress-state tests and the associated following items: (1) the failure surface for fully grouted but unreinforced specimens; (2) failure data and anisotropy; (3) elastic properties and anisotropy; (4) damping and strain-rate effects in the linear range; (5) the estimation of macroelement properties from component properties; (6) the influence of flaws, compaction, and admixtures on failure; and (7) the influence of reinforcing steel on the control of cracking and damage.

4.1 Materials

Typical component properties associated with the macroelements to be discussed are provided in Table 1 (for grout properties refer to column marked STD). Specimens were cut from fully grouted, 8x8-foot-walls. Grouting was accomplished in 8-foot lifts (pump). Compaction by puddling or vibration was conducted as indicated.

4.2 Failure Surface

Complete mapping of the failure surface of a macroelement in the stress space (N_{11}', N_{22}', N_{12}'), or the principal stress vs θ - space (N_{11}, N_{22}, θ) is a major undertaking. This problem is, however, alleviated by two factors; (1) extensive calculations concerning shear walls and other complex structures reveal that, in most applications, the normal stress on head joint planes is small when compared with normal and shear stress on bed joint planes, i e,

$$N_{11}' \ll N_{22}', N_{12}' \quad ; \tag{3}$$

and (2) experimental data shows a weak dependence of failure on the layup angle θ, i e, the composite under consideration is approximately isotropic (this point will be discussed later).

Table 1. Component Properties for Macroelements and Prisms.

	Block†	Mortar	Grout‡	
			STD	ADM
Compressive Strength (ksi)	3.97	2.42	4.03	4.34
	2.97	2.86	3.53	3.79
	3.27	2.39	3.51	3.41
	2.95	2.66	3.79	3.72
	3.41	2.83	4.15	3.66
	3.16	2.03	3.69	
	3.00	1.77	3.69	
	3.68		4.32	
			4.35	
			3.98	
			4.17	
			3.25	
mean	3.30	2.42	3.87	3.78
std. dev.	.37	.41	.35	.34
Tensile Strength (ksi)	310	229	247	
	291	253	253	
	373	162	324	
	294			
	297		240	
	363			
	377			
mean	329	215	266	
std. dev.	40	47	39	
Young's Modulus, Compression (psi)	2.5×10^6 (2.2-2.8)		2.6×10^6 (2.5-2.7)	
Young's Modulus, Tension (psi)			2.3×10^6 (2.1-2.5)	
Poisson's Ratio	.16 (.14-.18)		.16	

†Block: Type N, ASTM C90 Block; test coupons approx. 4.0" x 6.5" cut from face shells.

‡Grout: Coarse grout, ASTM C476 (6-sack grout)

A typical intersection of the material (macroelement) failure surface with the plane $N_{11}' = 0$ (see Section 2.5.1) is illustrated in Fig 10 for fully grouted but unreinforced specimens. The rays in these figures represent the layup angles and the corresponding proportional loading which results from the condition $N_{11}' = 0$ in equation (2), while equation (1) furnishes

$$N_{11} = - N_{22} \tan^2 \theta \ . \tag{4}$$

Data points, which represent statistical means of repeated tests, are denoted by circles and triangles. Stresses shown are based upon net cross-sectional areas.

Two basic failure modes were observed in these tests. In the tension zone, and in the compression zone for $|\theta| > 15$ deg, a brittle failure with a single crack was frequently observed, as illustrated in Fig 11a. ($\theta = -45$ deg). In the compression zone for $|\theta| < 15$ deg, failure appears to consist of multiple cracks, as shown in Fig 11b for $\theta = -10$ deg.

The curves in Fig 10 represent several macroscopic, analytical failure models considered to date. The dotted curve, shown for batch 6, is based upon the premise that failure occurs when a principal stress reaches either the tensile strength or the compressive strength associated with a uniaxial, 0 deg layup test. The solid curves result from the premise that the failure envelope in principal stress-space is linear in the tension-compression zone, as illustrated in Fig 12 for plain concrete under biaxial stress states. This model is seen to provide a more accurate description of material behavior. The two solid curves in Fig 10 correspond to estimated (from prism tests) compressive strengths, and measured (from 0 deg layup panels) uniaxial tensile strengths for two groups of specimens. Note that only two experiments are necessary for construction of this failure model: (1) the uniaxial tensile strength and (2) the uniaxial compressive strength. The dashed curve represents a modification of the solid curve for batch 6, to account for the anisotropy discussed below.

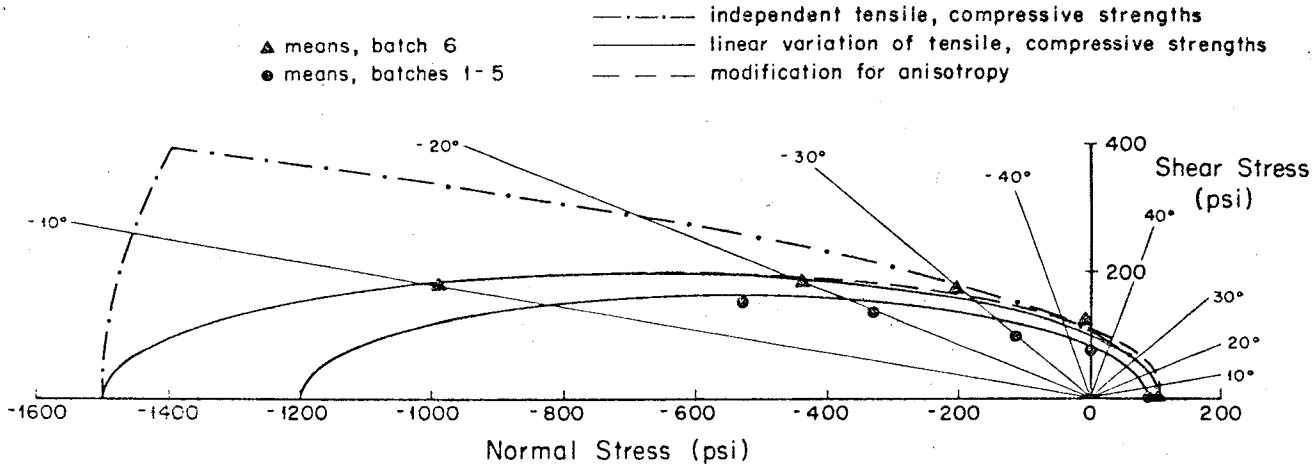

Fig. 10 Failure Envelope for Zero Head Joint Normal Stress.

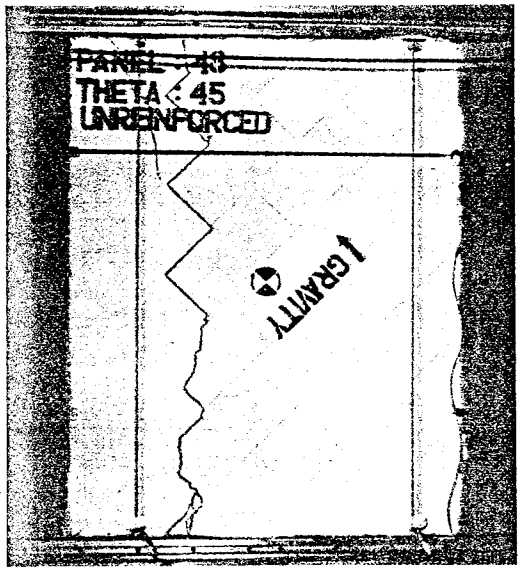

Fig. 11(a) Typical Joint Failure.

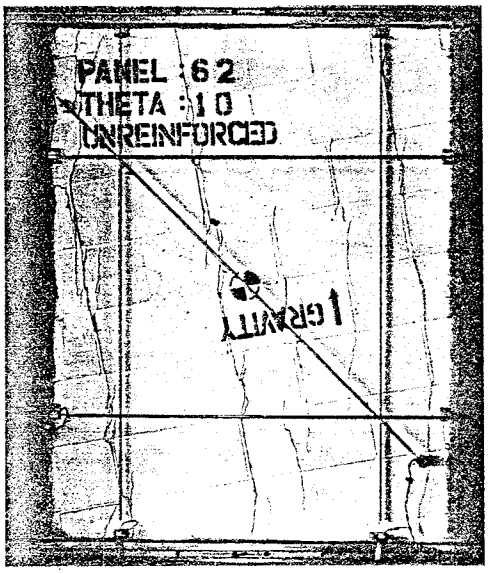

Fig. 11(b) Multi-Crack Failure.

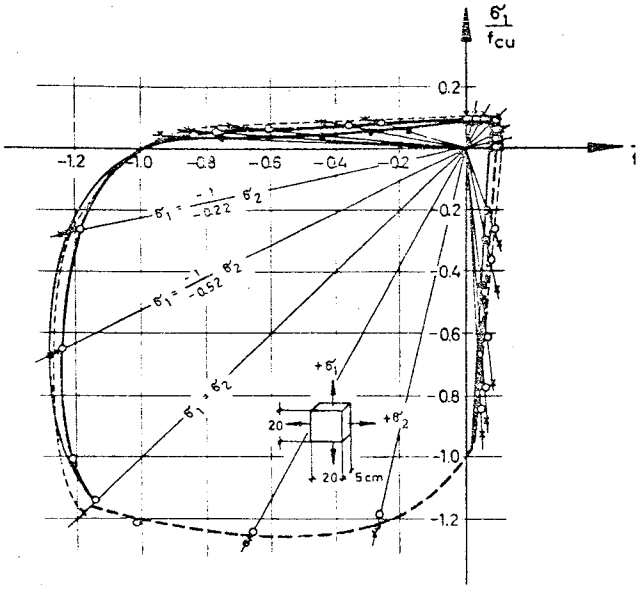

Fig. 12 Biaxial Strength of Concrete.

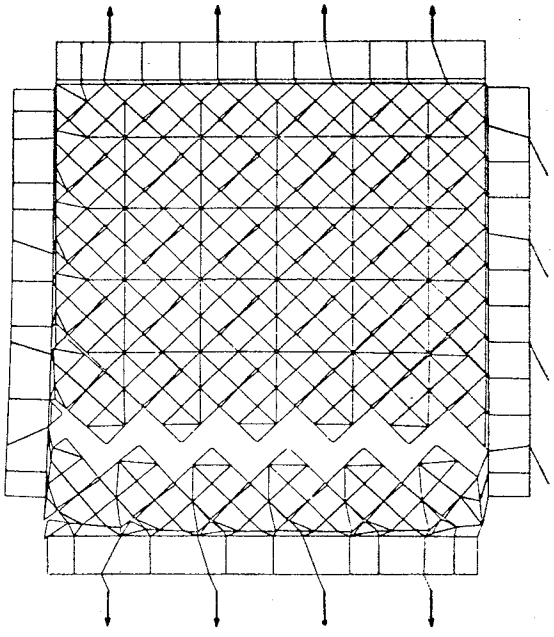

Fig. 13 Finite Element Prediction of Failure.

4.3 Failure and Isotropy

The above premise regarding the linear decrease of tensile strength in the presence of (principal) compressive stress is substantiated by Fig 14. Data on macroelement tensile failure indicates a slight increase in strength for layup angles near 45 deg, as shown in Fig 15, but the premise of material isotropy can be seen to hold within normal data-scatter for brittle materials of the type under consideration. For a layup angle of 0 deg, tension is applied to the bed joints. Each curve in Fig 15 represents a fit to the data of a second degree polynomial.

It should be noted that material anisotropy for a macroelement is a direct function of block and grout strengths. The strength combinations under study, by accident, led to an essentially isotropic material. The latter can be destroyed by a non-judicious selection of block and grout strengths. Estimation of material anisotropy from component properties is discussed in a later section.

4.4 Failure and Micro-modeling

It was noted above that a relatively elementary analytical model will suffice to predict failure. In more complex situations involving nonhomogeneous stress fields with large stress gradients and complex deformation fields, a more detailed analysis may be necessary. It is for this purpose that the micro-modeling is being pursued. Finite element simulations of panel behavior have been performed to assess the accuracy of current micro-modeling concepts. For this purpose the panel assembly is discretized into a system of plane stress finite elements. The grouted block and the adjacent mortar are represented by a single material whose properties are determined by a volume-based mixture procedure. The masonry joints are represented by an interface utilizing the interface technique discussed in reference [3]. Interface properties are determined from joint tests discussed in a subsequent section. A typical fracture pattern for a 45 deg uniaxial case is shown in Fig 13; this discretized system has 1674 degrees of freedom and a bandwidth of 154. The results of analysis performed to date, which were obtained by

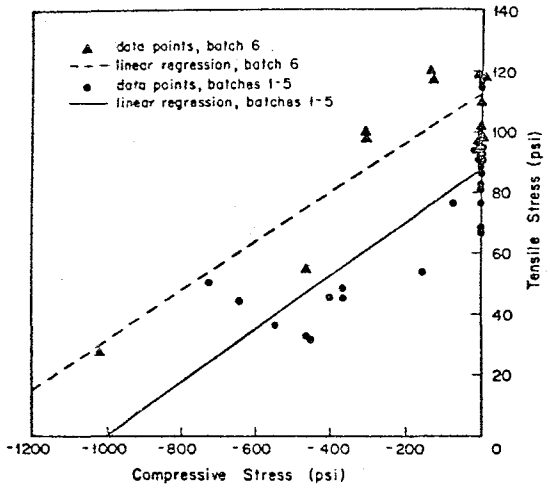

Fig. 14 Dependence of Panel Tensile Strength on Compressive Stress.

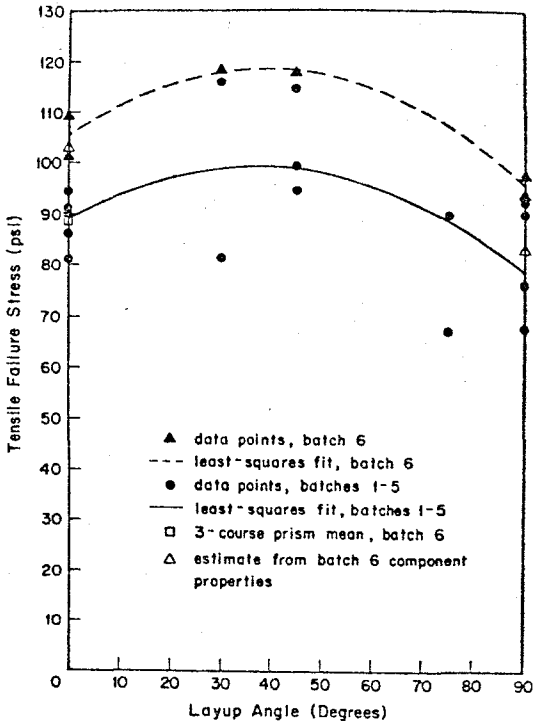

Fig. 15 Panel Tensile Strength Anisotropy.

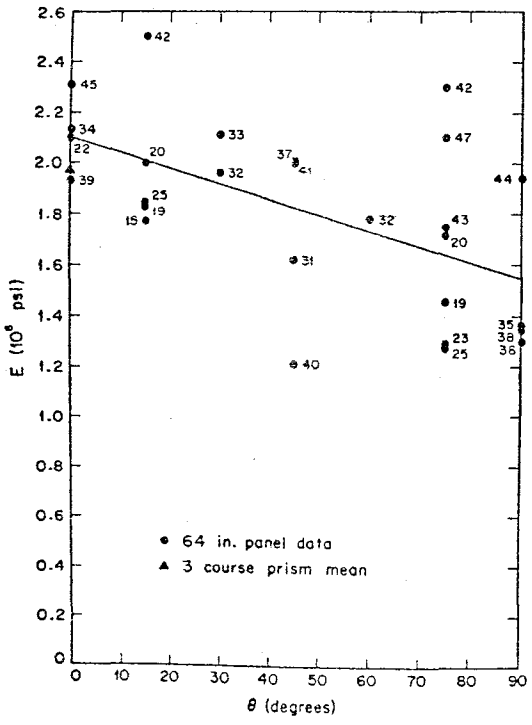

Fig. 16 Panel Stiffness Anisotropy.

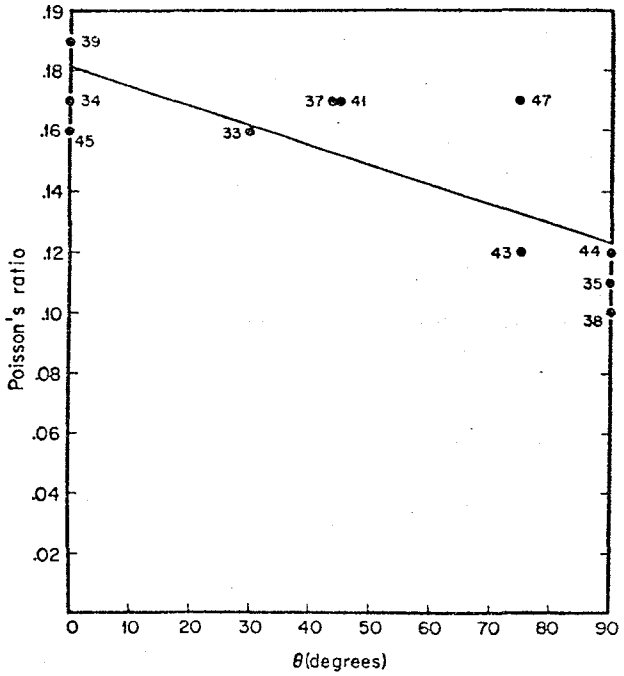

Fig. 17 Panel Poisson's Ratio Anisotropy.

using an out-of-core version of NONSAP, show excellent correlation with experimental data; for example, the ultimate strength of the model shown in Fig 12 was approximately 77 psi, compared to 80 psi obtained experimentally.

4.5 Elastic Moduli and Anisotropy

Typical variations of Young's modulus and Poisson's ratio with θ for the materials discussed above are illustrated in Figs 16, 17. This data was obtained via compression in the range 0-300 psi. A linear regression analysis of the data shows a clear trend wherein both moduli decrease form θ = 0 deg (compression across bed joint planes) to θ = 90 deg (compression across head joint planes). Since most specimens provide two data points (by reversing the roles of the principal stresses), one may observe this trend in the absence of data scatter by following the same specimen number in Fig 16. Compare, for example, θ = 15 deg with θ = 75 deg for specimens 19, 20, or 22 in Fig 16; or compare θ = 30 deg with θ = 60 deg for specimen 32.

While the data clearly indicates a degree of anisotropy, it is also clear that, for the materials under discussion, the material may be approximated as isotropic within the data scatter observed. This is an extremely important result.

4.6 Damping and Strain-Rate Effects

Figure 18 shows typical compressive cyclic stress-strain data (same specimen) ranging from a slight preload to approximately 250 psi for five strain-rates from .05 Hz to 2.0 Hz. Each figure depicits two cycles. Several extremely important observations regarding material behavior can be extracted from this data, which is typical.

First, the data clearly exhibits little or no strain-rate dependence over frequencies extending from essentially quasi-static to typical expected mode frequencies for full-scale structures [4]. Both slopes and hystersis loops remain invariant with frequency in the above range.

Second, the hystersis loops provide a measure of energy absorption or damping

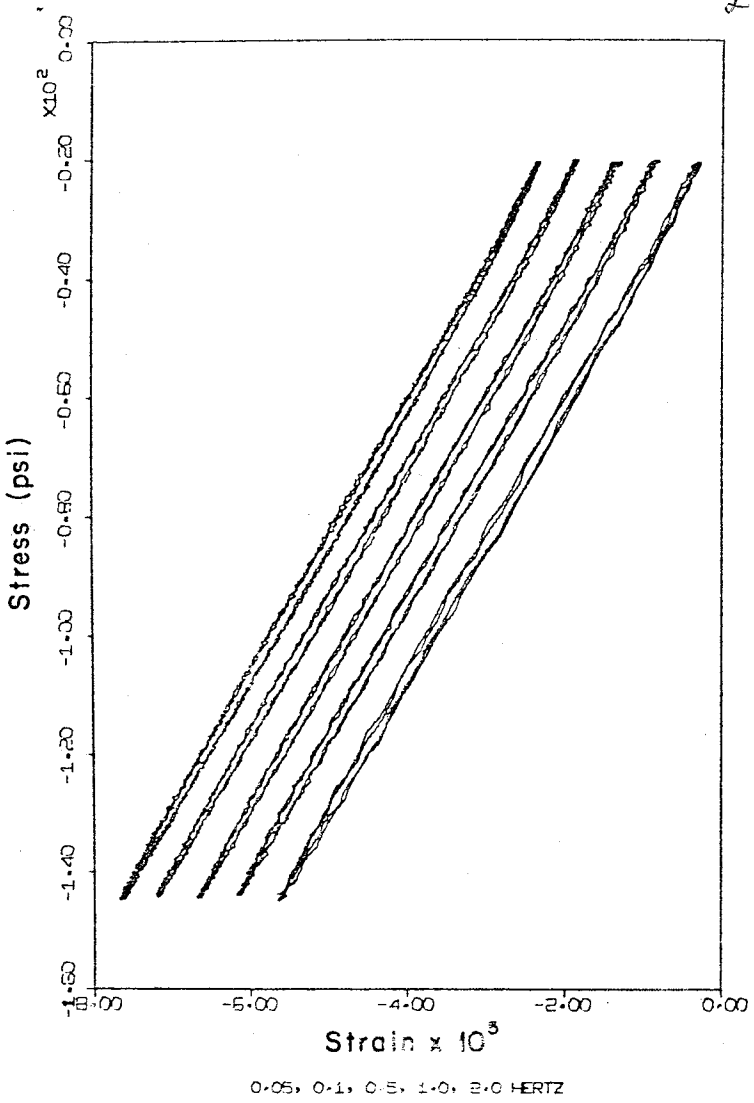

Fig. 18 Typical Panel Compressive Cyclic Data.

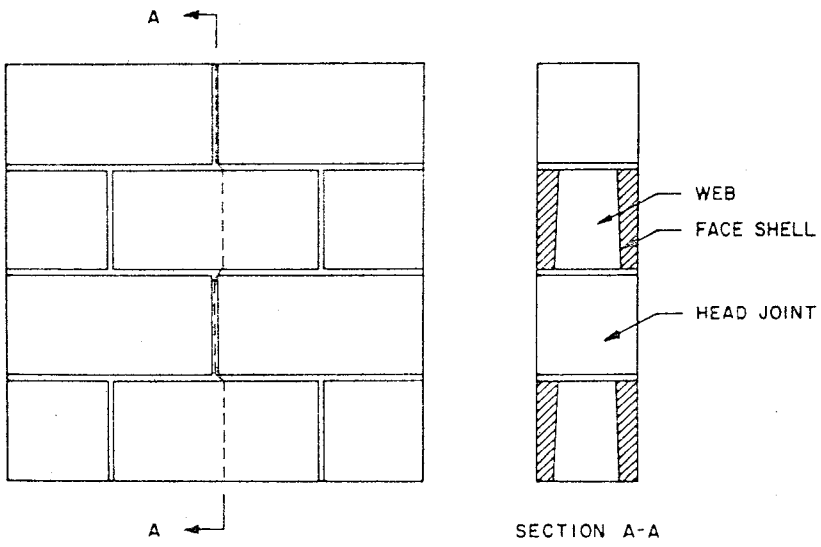

Fig. 19 Tensile Failure Pattern for 90 deg Layup Panel.

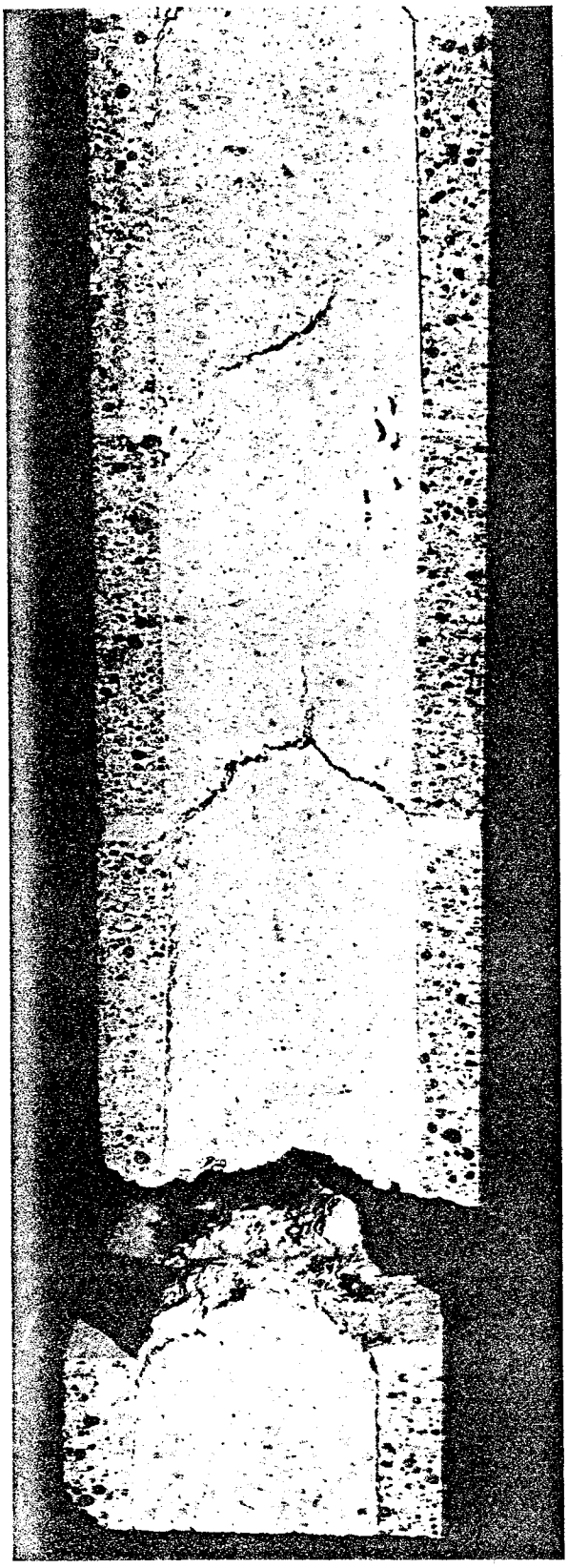

Fig. 20 Grout Bridges and Resulting Failure.

in the "linear elastic" material range. The fact that the areas of these loops do not depend upon frequency implies that material damping should not be modeled as viscous damping.

The implications of the foregoing observations may be serious. For example, the current earthquake response spectrum approach to the seismic design of buildings [5] is based upon the premise that the damping involved is of the viscous type. If the damping associated with a complete structure is the result of material behavior, then this premise is highly suspect in view of our findings. This potential problem is compounded by the fact that the response spectrum is highly sensitive to the damping assumed.

One may argue here that the first mode (or the first few modes) of a building performs as a narrow-band filter, and hence that one may approximate the structural damping mechanism as viscous wherein the damping factor is determined from data (logarithmic decrement) in the neighborhood of the modal frequency of interest. This approximation may suffice if conducted properly. Unfortunately, it does not appear that this has been the case in practice.

Consider, for example, the percent critical damping factors claimed in some masonry promotional literature [6]. Numbers ranging from 8 to 10 percent have been proposed for some masonry materials. Such information has evolved from the measurement of the rate of decay (logarithmic decrement) of material response to a transient blow from a hammer (in-plane), a steel-ball-pendlum impact [6] (out-of-plane), etc. Two things are wrong here. First, the response frequencies associated with such tests are too high-by several orders of magnitude in some cases; this results in artificially high damping coefficients (damping is known to be frequency dependent for sufficiently large frequencies). Second, and more important, the concept of critical damping has been incorrectly used. The latter is based upon the response of a single degree of freedom oscillator; the percent critical damping calculation necessitates a knowledge of the mass and frequency of this oscillator. If the oscillator is to be associated, e.g., with the first mode of vibration of a building, then the effective mass and frequency must correspond to this mode. That is, the percent critical damping is a function of the assumed mass, and the modal frequency.

It is of interest to estimate how far off the above mentioned 8 to 10 percent critical damping factors are - based upon the premise that such numbers orginate from the concrete masonry, and not from connections or non-structural elements. Consider Fig 18. If the damping is sufficiently small, the transient response to an initial value problem will be nearly harmonic. Suppose, as the data indicates, that material damping is independent of frequency. As in the case for viscous damping, the rate of decay curve is exponential and the decrement is a constant. The decrement for a macroelement can be calculated from Fig 18 by measuring the areas representing hysteresis and strain energy, and by computing the loss of strain energy per cycle. If this quantity does not depend on stress amplitude, then the decrement for a macroelement is the same as the decrement for a full-scale structure composed of the same material, i e, the energies of the subcomponents (macroelements) can be summed to yield the energies of the structure. Thus, one may now speak of a structural mode of vibration. The result? Critical damping factors of less than 2 percent are observed when the measured decrement is applied to an "equivalent" viscous model! Thus, if numbers such as 8-10 percent critical damping factors are to be employed in practice for concrete masonry structures, such high values must be the result of connection behavior, or some other aspect of the structure.

The above discussion concerned low stress amplitudes, i e, material response in the essentially linearly elastic range. Energy absorption and strain-rate dependence in the high stress regime is currently under study. In both cases, however, energy absorption and strain-rate dependence (if any) will be properly incorporated into the material constitutive relations.

4.7 Prediction of Macroelement Properties from Component Properties

From a practical standpoint, it is imperative that one be able to predict basic macroelement properties from component properties. Extensive testing has indicated that this is indeed possible. Several examples are provided below with respect to the failure surface described previously.

Consider the failure theory of Fig 10. This theory requires material isotropy and two data points: the uniaxial compressive and tensile strengths for, say, a 0 deg layup. The compressive strength may be determined from four or five-course prism data. Likewise, the tensile strength can be estimated by direct tensile testing of prisms. The above strengths may also be estimated from component properties.

Consider Fig 15. The open square, which represents the mean of repeated tests, is the result of a direct tensile - prism testing of "batch 6". This data is observed to provide a good 0 deg tensile strength estimate, and is conservative in that it lies below the actual macroelement (panel) data. (This is due to the increase in flaw sensitively with a decrease in specimen size).

The open traingle at 0 deg layup angle in Fig 15 is based upon the premise that (in the absence of bond beams), 0 deg tensile strength is determined solely by the grout tensile strength and grout area (no tensile strength is attributed to the mortar bond - a fact which has been substantiated by joint tests). The strength estimate is seen to be excellent.

The strength of a 90 deg layup specimen in tension is primarily a function of block strength. A typical failure pattern is illustrated in Fig 19. The head joints contribute little strength, and inspection of failed specimens revealed that most grout cores separated cleanly from the webs. But usually one web was failed , and adding that area to the area of the face shells gives the estimate of macroelement strength at 90 deg shown as the open triangle in Fig 15. The estimate is seen to be quite accurate. Whether the bonded area, and hence macroelement strength, can be predicted is being studied. Block strength here was determined by direct tensile testing of coupons sawcut from full-blocks.

The above two tensile strength estimates provide the necessary measure of anisotropy.

The estimate of macroelement compressive strength from the component properties is not quite so straightforward. The latter is currently under study.

It should be noted that a model for the statistical distribution of data from brittle

materials such as those under study requires a substantial number of macroelement tests for its development. No material description is, of course, complete without such a model.

Finally, an effort is also underway to predict elastic properties of macroelements from component properties. The latter will not be discussed here, however.

4.8 The Influence of Flaws, Compaction, Admixtures

Specimen sawcutting has afforded an unusual opportunity to observe flaws. Such cuts reveal much more information than cores, although cores are also taken in our tests.

To date some seventy macroelements have been tested. Virtually every specimen has exhibited flaws in the form of grout-block separation, voids, and most important - shrinkage cracks forming grout bridges. Figure 20 dramatically illustrates such flaws - and the fact that they can prematurely trigger failure.

With respect to block-grout separation - it is known that several mold release agents are used in the construction of concrete block. It is suspected that such agents adversely influence grout-block bonds. This matter is under investigation.

In an effort to mitigate the grout shrinkage/bridging problem, several grouting techniques are currently under study: (1) puddling of grout; (2) compaction and recompaction of grout via vibration; (3) and the use of grout admixtures with and without compaction. Figure 21 illustrates the influence of each technique on full-scale panels sawcut from 8X8-foot fully grouted walls. It can be observed that vibration compaction yields a specimen superior to puddling with or without admixture (the admixture in this case is Suconem G A (Grout Aid)).

Additional information on this subject can be found in Section 5.2.

4.9 The Influence of Reinforcing Steel

The influence of reinforcing steel in the control of macrocracking, and on the nonlinear, post macrocracking stress/strain range is of major concern in our studies.

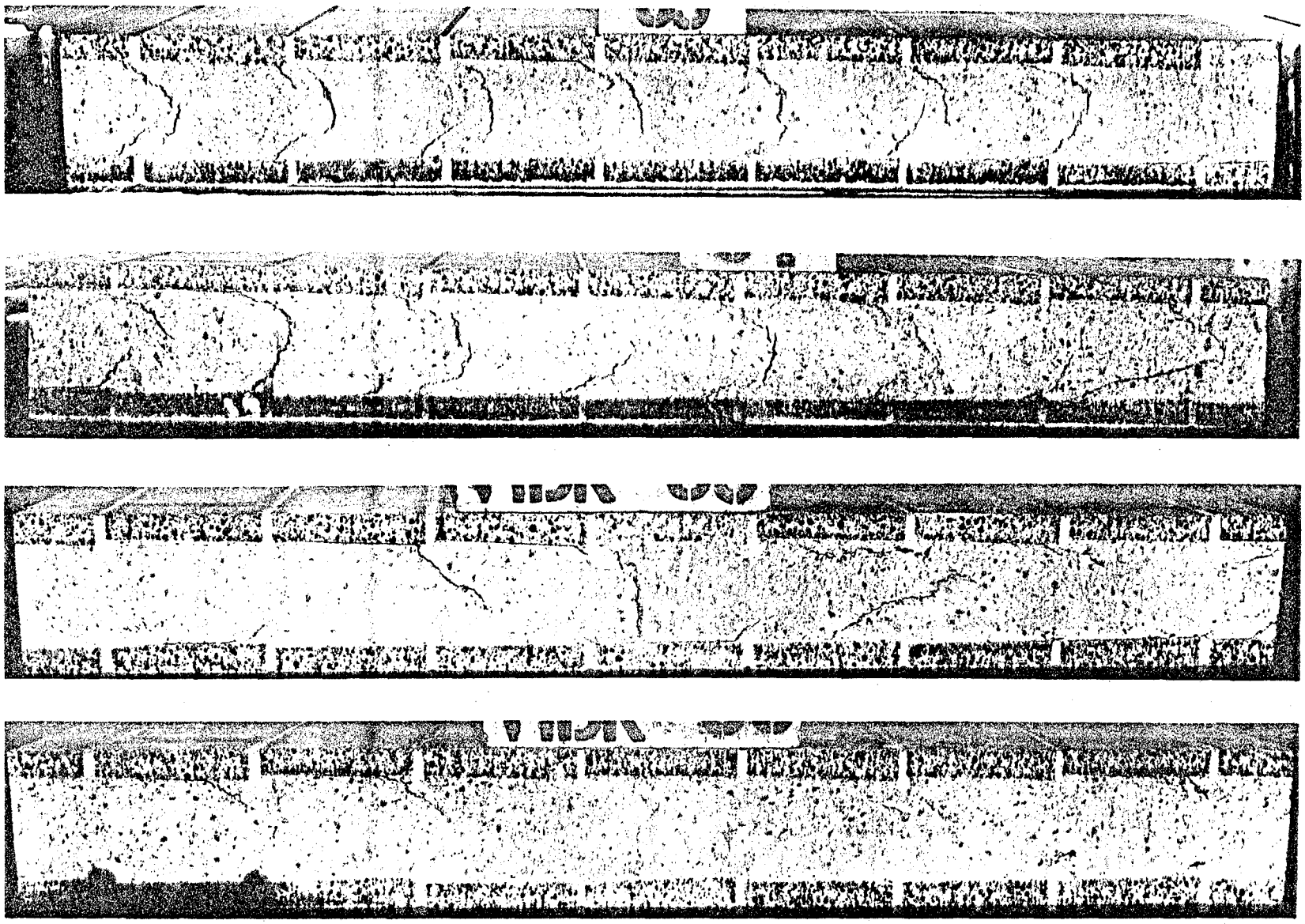

Fig. 21(a) Sides of Panels: Puddled; Admixture Puddled; Vibrated; Admixture Vibrated.

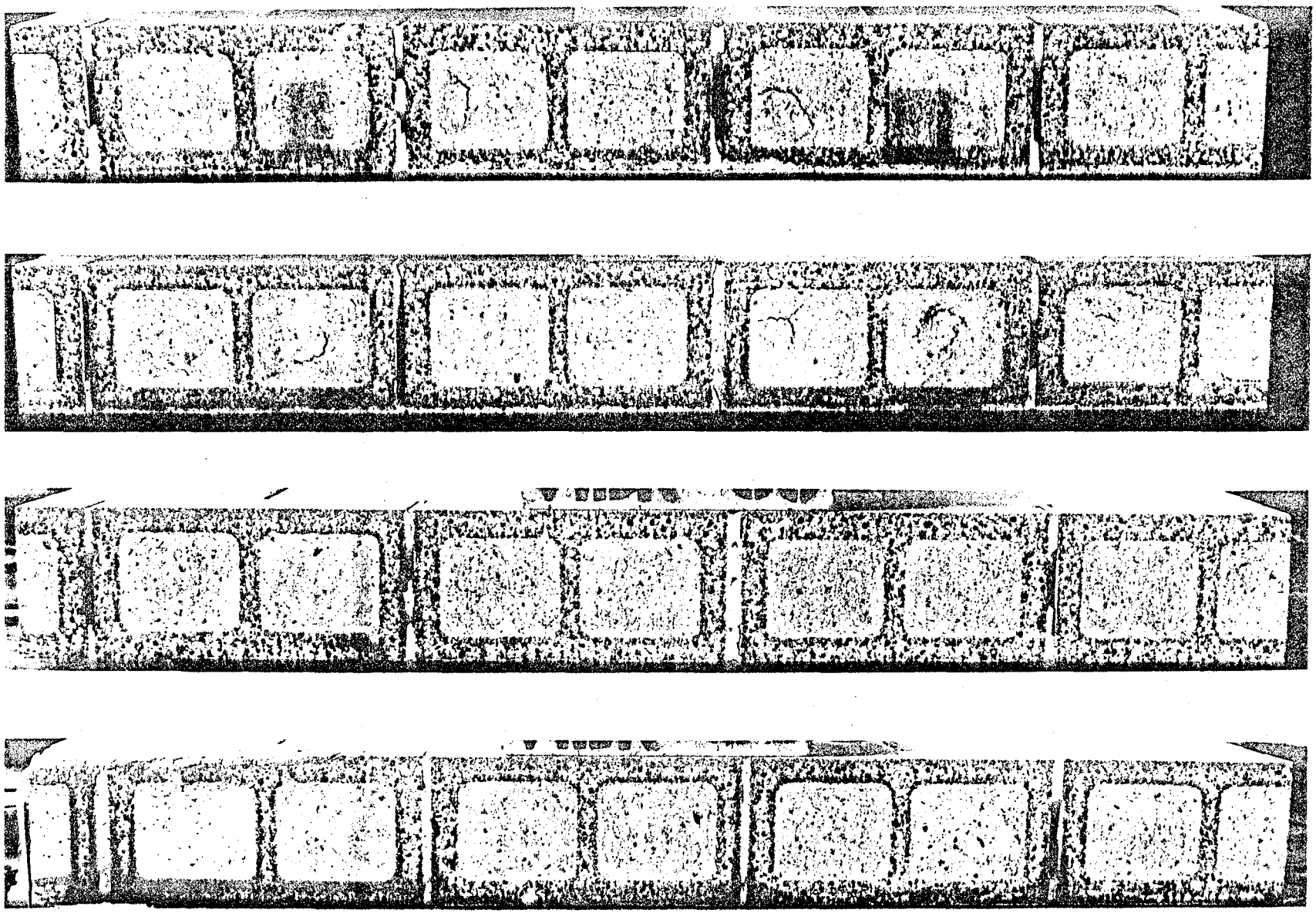

Fig. 21(b) Tops of Panels: Puddled; Admixture Puddled; Vibrated; Admixture Vibrated.

Current tests involve fully grouted specimens with two number five bars (grade 60) at 32 inches on center - both vertically and horizontally. The area of the steel in each direction is 0.6 in^2, whereas the net cross sectional panel area is 487 in^2; this yields a steel/masonry ratio of .00126 in each direction, which exceeds minimum UBC requirements.

The reinforced concrete masonry tests are currently in a production mode, and it is perhaps premature to discuss results. However, several items are noteworthy:

First, the initial macrocracking stress level does not appear to be significantly influenced by steel/masonry ratios of the magnitude under discussion. Thus, failure envelopes, Fig 10, as determined from unreinforced tests should predict the onset of macrocracking.

Second, under monotonically increasing strain, a substantial drop in the macroelement stress occurs at the onset of macrocracking, i e, the load-carrying capability dramatically decreases. This is illustrated in Fig 22 for a typical 0 deg uniaxial test under displacement control. This drop is associated with load transfer from masonry to steel, and the fact that the steel area is not sufficient to maintain the original load without considerable extension.

Third, upon continued straining of the specimen, reloading is observed - the slope of which is smaller than that of the masonry, but larger than that associated with the steel alone. This implies that the load is shared by both steel and masonry.

Fourth, upon cyclic straining from zero to a tensile strain, stiffness degradation can be observed, Fig 22. This degradation is associated with multiple cracking (see Fig 23) in contrast to a single crack observed at the failure point of unreinforced specimens. (The crack marked "1" denotes the initial macrocrack associated with the peak load of Fig 22).

It is clear at this stage of research that the amount of steel utilized in most construction is not sufficient to prevent an unstable branch of the stress-strain curve associated with a reinforced macroelement.

In passing, it is noted that specimen fixturing was designed to provide a uniform

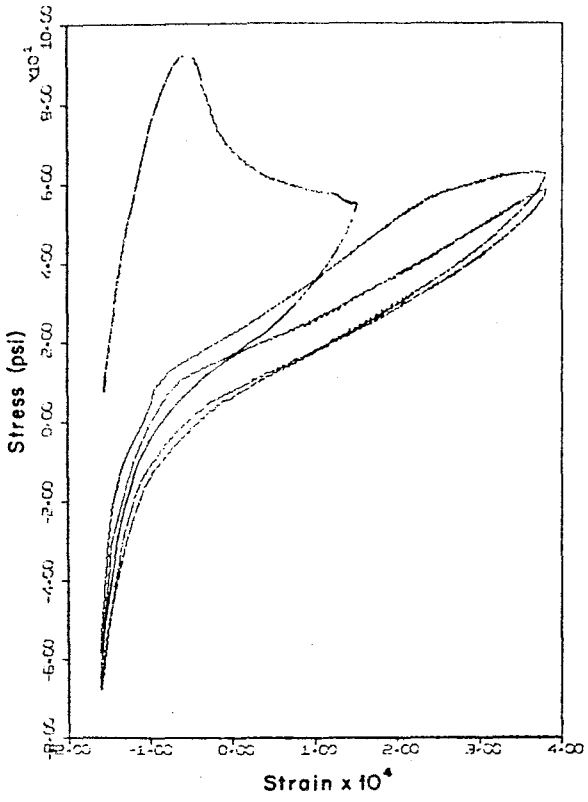

Fig. 22 Reinforced Panel Failure and Post-Failure Cycling.

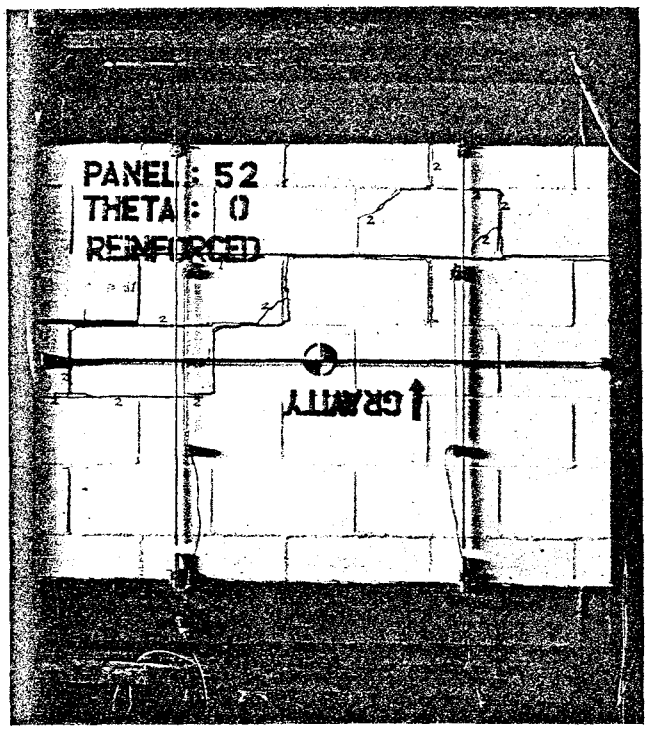

Fig. 23 Multiple Cracking of Reinforced Panel.

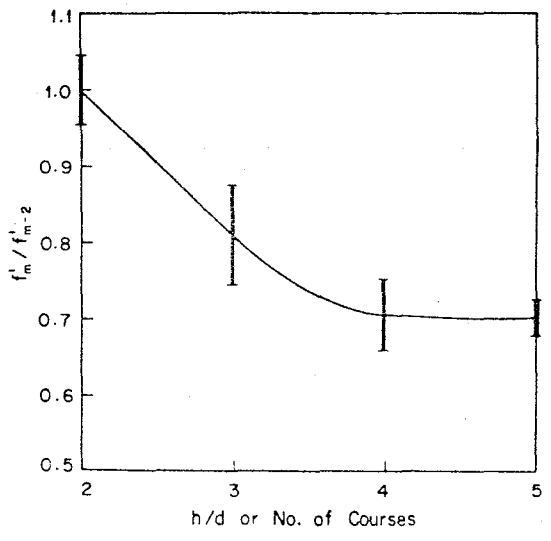

Fig. 24 Correlation of Prism Strength and Geometry.

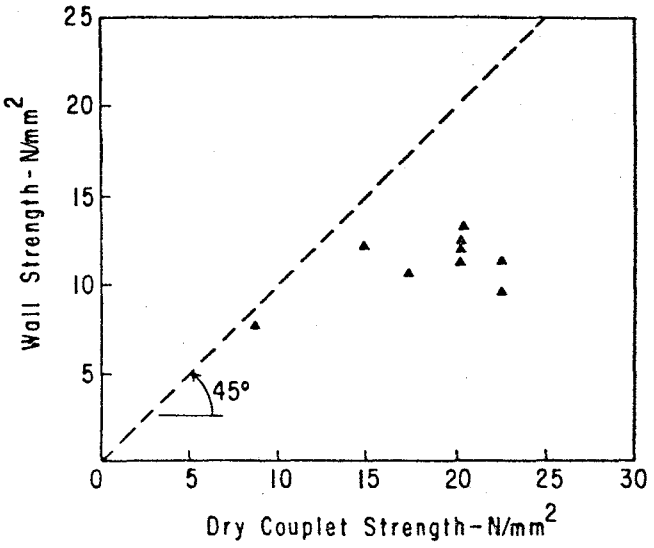

Fig. 25 Comparison of Ungrouted Wall and Couplet Strengths.

strain field in both steel and masonry prior to macrocracking. Proper loading of the steel is not a trivial matter experimentally, and no attempt will be made here to explain the fixture details.

V. SELECTED RESULTS - PRISMS

Once again, a complete description of small-scale tests is beyond the scope of this paper. Below, representative tests and sample results are provided in order to give the reader a proper perspective of the program.

5.1 Influence of Number of Courses on Strength

Present working stress and design methods are based primarily upon a knowledge of the masonry compressive strength, f'_m. In practice, f'_m is usually determined by prism tests. Current masonry codes and design recommendations (see reference [1]) either explicitly or implicitly recommend that f'_m be computed on the basis of 2-course prisms laid in stacked bond, and capped according to ASTM C140 wherein a sulfur fly-ash compound or a high strength gypsum plaster is used. Test procedures correspond to ASTM E447. Code correction factors purport to enable conversion of the strength of a particular geometry to that of a standard prism. A UBC correction factor of unity is presently applied to the 2-course prism ($h/d = 2.0$). This evidently implies that a strong correlation with $h/d = 2.0$ and full-scale masonry exists. Our research clearly indicates this premise to be false and nonconservative. In particular, test data indicates that prism strength is significantly influenced by load-platen restraint and, in the absence of a soft capping material, is a strong function of the number of courses-up to four-to-five courses. A typical example is illustrated in Fig 24. The data was obtained from full-block, fully grouted specimens; precision cutting to the desired h/d ratio was utilized in place of a high-strength capping material. The bearing platens at each end consisted of solid 8x8x16-inch aluminum blocks. Platen restraint resulted in a shear-mode failure in 2-course prisms, and combined shear-tensile splitting in 3-course prisms. Proper

tensile splitting was observed in 4 and 5-course prisms. Based upon the 5-course data, the 2-course results are approximately 50 percent too high. Also, the data indicates that prism strength is a function of the number of joints in the specimen as well as the h/d ratio. Finally, an extensive literature review (see Reference [1]) revealed an amazing fact: Virtually all code correction factors for prism geometry are based upon a common source - the preliminary and exploratory investigation by Krefeld in 1938 (see reference [1]) - on brick! This is patently unjustified. A correlation of Krefeld's work with a number of codes is shown in Table 2 (each code is based upon a different "standard" prism geometry-hence the normalization factor may be different). In view of the above discussion, one would expect poor correlation between 2-course prism and wall data; this is demonstrated by tests by Read and Clements on ungrouted walls, Fig 25 (see Reference [1]). The component materials for the specimens discussed above are described in Table 3.

5.2 Influence of Compaction, Admixtures on Compressive and Tensile Strengths

The extensive flaws observed in full-scale masonry led to a comprehensive study of the influence of compaction and/or admixtures on flaws-and hence on strength. One such study is briefly described below. The component properties associated with these tests are described in Table 1.

Table 4 compares compressive strengths obtained from 4-course prisms (full block, fully grouted, stacked bond) consisting of four test types: (1) puddled grout (marked STD); (2) vibrated grout (marked STD VIBR); (3) puddled grout with an admixture (Suconem G A or Grout Aid; marked ADM); and (4) vibrated grout with an admixture (Grout Aid; marked ADM VIBR). A significant difference was observed between puddled and vibrated specimens; the former was only 66 per cent as strong as the latter. The addition of grout aid in these tests appears to improve strength - with or without vibration. This last point is being reexamined for small-scale specimens, and a panel test-series is underway to verify the influence of Grout Aid in full-scale masonry.

Table 2. Comparison of Correction Factors for Prism Shape after "Code Factor" Modification.

Source	"Code factor"	h/d= 1.5	2.0	2.5	3.0	4.0	5.0	6.0
Krefeld	—	0.59	0.67	0.75	0.80	0.89	0.96	1.00
New Zealand Standard	1.50	0.58	0.67	0.74	0.80	0.89	0.95	1.00
Australian Standard	1.25	—	0.68	0.74	0.80	0.88	0.93	0.93
Canadian Code (concrete)	1.50	0.57	0.67	0.74	0.80	—	—	—
Canadian Code (brick)	0.93	—	0.68	0.74	0.80	0.89	0.93	—
Uniform Building Code	1.50	0.57	0.67	0.74	0.80	—	—	—
National Bureau Standards	1.50	0.57	0.67	0.74	0.80	—	—	—
Structural Clay Prods. Inst.	0.93	—	0.68	0.74	0.80	0.89	0.93	—

Table 3. Component Properties for Prism Geometry and Interface Tests.

		Block	Mortar	Grout
Compressive Failure Stress		2080	3780	5380
		2320	4580	5780
		3260	3780	5770
		2570	4260	
		3320		
		2450		
		3210		
		3210		
		2680		
		2400		
	mean	2750	4100	5640
	std. dev.	460	390	230
Young's Modulus† (10^6 psi)		1.74	0.86	1.68
		1.47	0.98	2.13
		1.89	0.81	1.44
			0.85	1.83
	mean	1.70	0.88	1.77
	std. dev.	.21	0.07	.29

†Tension for block, compression for mortar and grout

Table 4. Compressive Strength for 4-Course Grouted Prisms.

	STD	STD VIBR	ADM	ADM VIBR
Failure Stress f_c (psi)	1348	2274	2181	2004
	1449	2426	2350	2282
	1398	2089	2324	2173
	1887	2434	2308	2148
	1490	2358	2450	2468
mean	1524	2316	2323	2215
std. dev.	212	142	96	173

Table 5. Tensile Failure Strength for 3-Course Grouted Prisms.

	STD	STD VIBR	ADM	ADM VIBR
Failure Stress f_t (psi)	69.7*	116.3*	92.5*	94.8*
	111.2	91.8	110.7	98.6
	111.2	127.3*	118.3	116.3
	84.3*	113.0	110.4	143.2
	69.9	89.9	95.8	107.4
mean	89.3	107.7	105.5	112.1
std. dev.	20.9	16.3	10.9	19.3

*Polymer bond (all others epoxy bond)

Table 6. Ratio of Prism Tensile to Compressive Strength.

	STD	STD VIBR	ADM	ADM VIBR
f_t/f_c	.059	.047	.045	.051

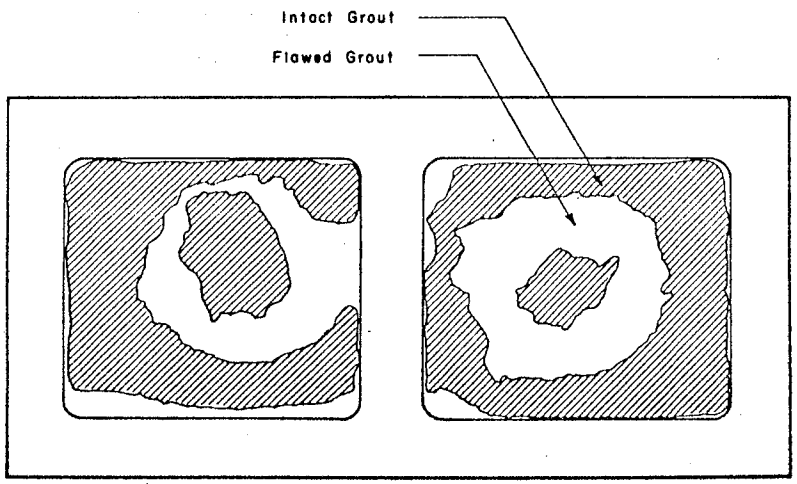

Fig. 26 Grout Flaws at Bed-Joint Plane.

Table 5 compares tensile strengths (measured directly from 3-course prisms laid in stacked bond and fully grouted). Again, it is evident that vibration compaction is significantly superior to puddling. Admixture tests are under reevaluation, as noted above.

5.3 Ratio of Tensile to Compressive Strengths

The tensile strength of plain concrete is approximately 0.1 times the compressive strength. The data of Table 6, obtained from the foregoing test series, shows that the ratio of tensile to compressive strength for concrete masonry (referred to bed joint planes) is approximately 0.05. The reason? The mortar bonds furnish virtually no tensile strength, the grout core takes the tensile load, and the ratio of grout area to the total cross sectional area is approximately a factor of two.

5.4 Influence of Flaws

The influence of flaws is implicitly exhibited in the data of Tables 4 and 5. That is, vibration compaction and admixtures tend to reduce the number of flaws and hence to increase strength.

An explicit, dramatic flaw influence, however, is worth noting at this point. Upon examination of the surface associated with a failed, puddled prism (failed in tension) with no admixture, the cross-hatched area of Fig 26 was deduced to be free from flaws, i e, the remaining area represented a flaw in which no bond existed across the plane of failure. Based upon the measured tensile strength of the grout, and the measured area of integrity, the tensile strength of the prism was predicted exactly. Hence there can be no doubt that flaws significantly influence masonry strength.

It should be noted that a definite scale effect has been observed with respect to flaws. This point, which was mentioned under Section 4.7 is such that small specimens, such as prisms, are more flaw sensitive than full-scale specimens, such as panels.

5.5 Elastic Moduli

Typical initial tangent moduli based upon the 3-course tension tests described previously are shown in Table 7. These data are in good agreement with full-scale panel data. Failure-point secant moduli are also provided in Table 8. Measurements were conducted as illustrated in Fig 27.

Of considerable interest, from the standpoint of nondestructive testing, is the ratio of moduli to strength. Typical data on this subject is provided in Table 9.

5.6 Prediction of Compressive Strength from Component Properties

Whereas the tensile strengths of either prisms or panels can be estimated from component properties, Tables 3 and 4 indicate that the situation is not as simple for the case of compression. Note that the component compressive strengths in Table 1 exceed the prism compressive strength. This matter is currently under investigation.

VI. SELECTED RESULTS - INTERFACES

6.1 Materials

The component materials for this test series are described in Table 3. Grouted specimens were compacted by puddling.

6.2 Joint Behavior

Data on joint fracture and post-fracture behavior is a prerequisite to a basic understanding of failure processes, and is necessary for modeling on the micro-scale. A typical test-setup for monotonic loading of full-blocks is illustrated schematically in Fig 28. In each test a constant normal stress was maintained across joint-planes, and the shear-stress distribution on these planes was varied by driving the center block in displacement control. Figures 29 and 30 exemplify typical static and dynamic[7] behavior

[7] The dynamic test fixture is complex and is not shown here.

Table 7. Initial Tangent Modulus for Prism Tension Test.

	STD	STD VIBR	ADM	ADM VIBR
$E_T(10^6$ psi)	1.86	2.13	2.14	2.27
	2.01	2.04	1.96	1.92
	1.97	1.97	2.12	2.12
	1.43	2.13	1.87	1.99
	1.56	2.10	1.80	2.05
mean	1.77	2.07	1.98	2.07
std. dev.	.26	.07	.15	.13

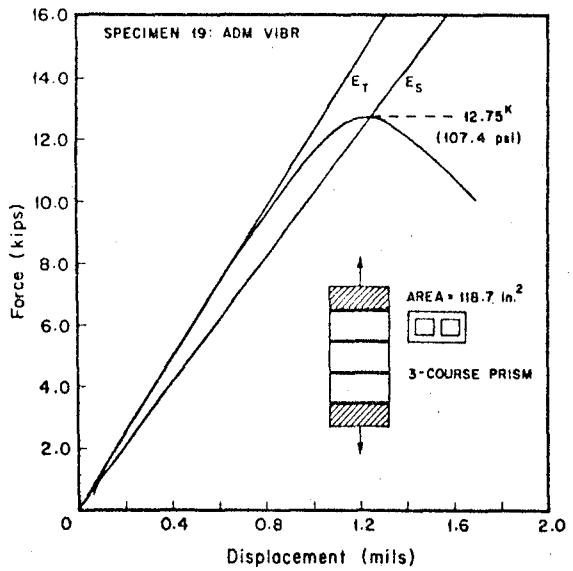

Fig. 27 Typical Prism Tensile Failure Test.

Table 8. Failure - Point Secant Modulus for Prism Tension Test.

	STD	STD VIBR	ADM	ADM VIBR
$E_S(10^6$ psi)	1.17	1.37	1.57	1.56
	1.51	1.26	1.70	1.33
	1.36	1.29	1.87	1.64
	1.10	1.68	1.66	1.59
	1.20	1.42	1.63	1.73
mean	1.27	1.40	1.69	1.57
std. dev.	.17	.17	.11	.15

Table 9. Ratio of Prism Strength to Initial Tangent Modulus for Tension Test.

	STD	STD VIBR	ADM	ADM VIBR
$\frac{f_t}{E_T} \times 10^6$	37.5	54.6	43.2	41.8
	55.2	45.0	56.5	51.4
	56.5	64.6	55.8	54.9
	58.9	53.1	59.0	72.0
	44.8	42.8	53.2	52.4
mean	50.6	52.0	53.5	54.5
std. dev.	9.1	8.7	6.1	11.0

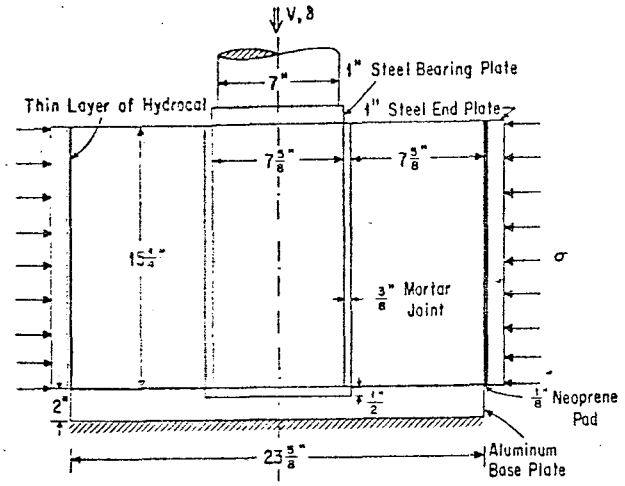

Fig. 28 Joint Test Setup.

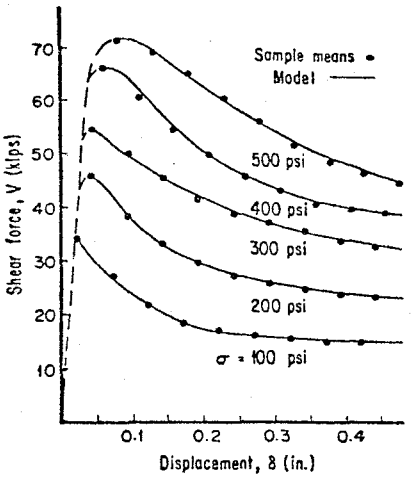

Fig. 29 Behavior of Bed Joints Under Precompression.

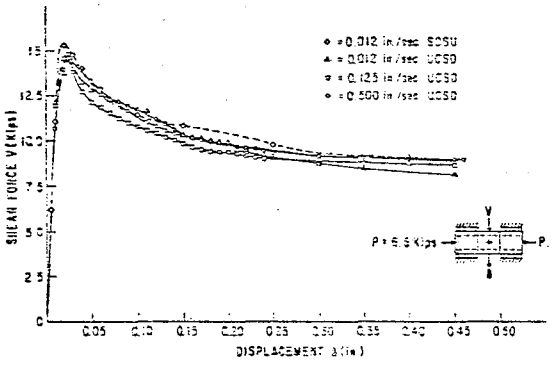

Fig. 30 Strain-Rate Dependence.

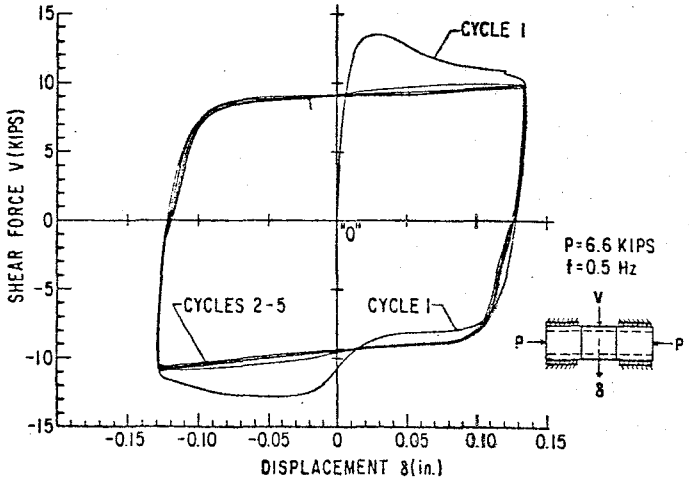

Fig. 31 Joint Behavior Under Cyclic Loading.

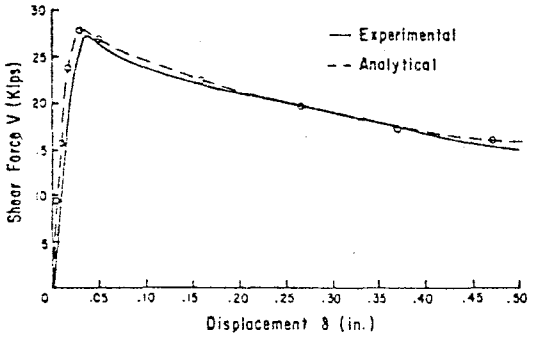

Fig. 32 Finite Element Simulation of Joint Behavior.

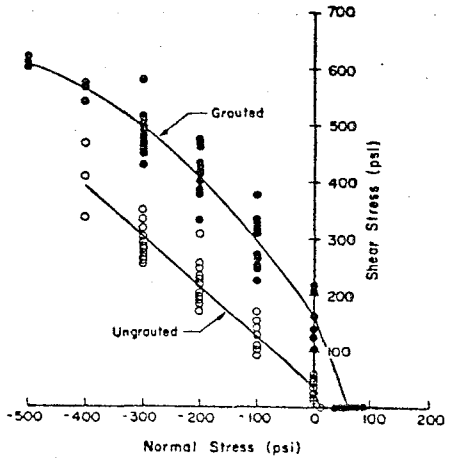

Fig. 33 Dependence of Joint Maximum Shear Stress on Normal Stress.

for grouted and ungrouted bed joints. The following basic characteristics are noted: (1) joint fracture strength increases monotonically with precompression up to a block-failure transition (the maximum shear stress vs normal stress for both grouted and ungrouted specimens is shown in Fig 33); (2) under precompression exceeding 100 psi-fracture load decreases with displacement (Fig 29) in a relatively smooth manner to a limiting value which, in turn, depends upon the level of precompression; (3) no discernible rate-dependence is evident in the ranges .01 to .50 in/sec under monotonic loading (Fig 30) and in the range .05 to .50 Hz under cyclic loading; (4) cyclic experiments (Fig 31) indicate that, following the first load reversal, load-displacement history is a function only of total displacement-path length and is not direction-sensitive; (5) ultimate strengths of head joints, and ungrouted bed joints are considerably less than associated grouted bed joints; (6) in the absence of precompression, joint behavior is brittle - ungrouted bed and head joints exhibit extremely low (3-30 psi) shear and tensile strengths as well as large data-scatter.

Joint shear force V vs displacement δ data suggested that the post-fracture regime could be represented by solutions of the differential equation

$$dV/d\delta = - c[V(\delta) - V_\infty] \tag{5}$$

where V_∞ denotes the asymptote at "infinite" displacement and c is a function of the work $W(\delta)$ done up to the displacement δ, viz,

$$W(\delta) = \int_{\delta_1}^{\delta} V(\delta')d\delta' . \tag{6}$$

Using the following solution of (5),

$$[W(\delta) - V_\infty]/[V_1 - V_\infty] = \exp[-\{\bar{c}\int_{\delta_1}^{\delta} [W(\delta')]^{1/3}d\delta' + b\}] \tag{7}$$

where δ_1 corresponds to the maximum shear for V_1, a nonlinear regression method was developed to determine the constants $\bar{c}$, b, and v_∞, and the correlation shown in Fig 29 was obtained. The points denote statistical means from at least three tests. Agreement is remarkable.

Finite element simulation of the joint tests was performed as a first step in the micro-modeling process. Local properties were established which enabled the analysis to match the experimental V vs δ data and which are reasonable when judged against independent measurements of interface strength. A typical correlation for ungrouted bed joints is shown in Fig 32. Agreement is seen to be good. Details of this work are contained in reference [3]. Subsequent to "tuning" the simulation of joint data, the above finite element model was utilized to predict biaxial panel behavior without further "tuning".

VII. CLOSURE

The program described, in part, herein represents the first fundamental and comprehensive effort to describe the material properties of concrete masonry.

The experimental apparatus necessary to generate data with integrity is, of necessity, complex and sophisticated. A time span of approximately two years has been necessary to bring all systems to a production basis. An avalanche of important results is now taking place.

While modeling was not discussed, excellent correlation has been obtained to date between experimental results and finite element simulations or modeling on the micro scale. In particular, it appears that the macro-behavior of concrete masonry can be rationally predicted from masonry constituent properties.

Finally, masonry is some 20 years or more behind concrete with respect to knowledge of material properties. Such a gap cannot be closed overnight. It is imperative that programs of the type discussed in this paper be sustained for a time period sufficiently long to allow the effort to come to fruition.

It is also imperative that the masonry industry organize on a national basis - much as the concrete industry has - if progress in this area is to be made within a reasonable time period. The absence of comprehensive knowledge concerning fundamental material properties - if allowed to continue - can only invite potentially enormous safety and economic problems.

REFERENCES

1. Hegemier, G. A., "Mechanics of Reinforced Concrete Masonry: A Literature Survey," Report No. AMES-NSF-TR-75-5, University of California, San Diego, 1975.

2. Mays, R. L., and R. W. Clough, "A Literature Survey - Compressive, Tensile, Bond and Shear Strength of Masonry," Report No. EERC 75-15, University of California, Berkeley, 1975.

3. Arya, S. K., "A Method for Incorporating Interface Discontinuities in Finite Element Analyses with Application to Concrete Masonry Rheology," Weidlinger Associates Report No. R-7522, prepared for the University of California, San Diego, 1975.

4. Krishnamoorthy, G., G. A. Young, and G. A. Hegemier, "Prediction of the Torsional Response of a Multistory Reinforced Concrete Masonry Building by a Three-dimensional Dynamic Analysis," Proceedings of Fifth World Conference on Earthquake Engineering, Vol. 1, No. 13, Rome, 1973.

5. An Evaluation of Response Spectrum Approach to Seismic Design of Buildings, A Study Report for Center for Building Technology, Institute of Applied Technology, National Bureau of Standards, Washington, D. C., 20234, by Applied Technology Council (ATC-2), San Francisco, California, September, 1974.

6. Dickey, W. L. and R. W. Harrington, Report "The Shear Truth About Brick Walls," Western States Clay Products, Assoc., Inc., San Francisco, Calif., 1970.